

A Subsystem Ginzburg-Landau and SPT Orders Co-existing on a Graph

Jintae Kim,¹ Hyun-Yong Lee,^{2,3} and Jung Hoon Han^{1,*}

¹*Department of Physics, Sungkyunkwan University, Suwon 16419, Korea*

²*Department of Applied Physics, Graduate School, Korea University, Sejong 30019, Korea*

³*Division of Display and Semiconductor Physics, Korea University, Sejong 30019, Korea*

(Dated: January 5, 2022)

We analyze a model demonstrating the co-existence of subsystem symmetry breaking (SSB) and symmetry-protected topological (SPT) order, or subsystem LSPT order for short. Its mathematical origin is the existence of both a subsystem and a local operator, both of which commute with the Hamiltonian but anti-commute between themselves. The reason for the exponential growth of the ground state degeneracy is attributed to the existence of subsystem symmetries, which allows one to define both the Landau order parameter and the SPT-like order for each independent loop.

I. INTRODUCTION

Multiply degenerate ground states in a many-body system are usually generated as a consequence of global symmetry breaking (GSB). A prime example of GSB is the twofold degeneracy of the ground states in the Ising model, where all spins are either up or all down. One of the remarkable advances in condensed matter theory over the past decades is the identification of a new mechanism by which multiple ground state degeneracy (GSD) is generated. One of these routes is the topological order, as most dramatically realized in fractional quantum Hall systems^{1,2}. Another recently discovered path to having multiple GSD is the so-called SPT order³⁻⁷. In models with SPT order, the ground state is unique if defined on a closed manifold but becomes multiply degenerate on an open geometry such as the open chain. Among the tell-tale signs of SPT order is the symmetry fractionalization of the global symmetry at the edges⁸⁻¹¹ which is also responsible for the multiple GSD. A lot of different models exhibiting SPT order has been examined in the past, in particular in one dimension¹²⁻¹⁴. Some models demonstrate the GSB even for the closed geometry, together with the SPT order^{12,14}. A recent twist to the original idea of SPT order protected by the global symmetry is the subsystem SPT (SSPT), being protected by the symmetries in a sub-manifold of the overall system¹⁵.

The SPT models treated in the past considered an alternating site and link variables arranged in a one-dimensional fashion. The case of m degrees of freedom residing on the vertices and n degrees of freedom on the links was considered in Refs. 16–19. The model exhibited a multiple GSD even for a closed chain. When the same model was placed on a graph, the GSD increased exponentially with the number of holes, called the first Betti number, in the graph. In this paper, we give a clear interpretation of the results found in Ref. 19 in terms of the notion of subsystem Landau and SPT orders. Features that are characteristic of symmetry breaking as well as SPT can be found in this model, and for each closed loop in the graph. We label such order as the subsystem Landau-SPT order, or SLSPT order for short. The observation of the co-existence of Landau and SPT orders

in a given chain had been made in the past^{12,14}, but not been extended to the case of a general graph. In Sec. II we review the V_2/L_4 model introduced in Ref. 19, which is a generalization of the V_2/L_2 model (to be defined precisely) studied by several authors in the past^{13,14,19}. The ground state degeneracy this model is understood in terms of a properly defined Landau order parameter in Sec. III. The V_2/L_4 on a graph is analyzed in terms of the co-existing Landau and SPT orders in Sec. IV. The origin of the exponential growth of GSD is understood. We make a summary and conclude in Sec. VI.

II. V₂/L₄ MODEL

For self-consistent reading of this paper, we make a brief review of the V_2/L_4 model introduced in Ref. 17 and analyzed in Ref. 19. In a family of Hamiltonians we will call the V_m/L_n model, there reside m degrees of freedom, or levels, at the vertices (v) and n levels at the links (l). In the simplest case of a one-dimensional chain, the vertices and links appear alternatively, as illustrated in Fig. 1. Quantum states at the vertices and links are written $|\alpha\rangle_v$ and $|\beta\rangle_l$, with $0 \leq \alpha \leq m-1$ and $0 \leq \beta \leq n-1$, respectively.

The Hamiltonian of the V_m/L_n model is a sum of mutually commuting projectors. One type of projector called A_v is defined with respect to a vertex, while the other type C_l is defined with respect to a link. Their specific expressions depend on the choice of (m, n) representing the respective dimension of the Hilbert space at the vertices and links. It turns out the $m = n = 2$ case had been studied extensively in the past^{13,14}. Our focus here is on the extension to $n > 2$. Striking differences from the V_2/L_2 situation already show up for the V_2/L_4 case, where we will be devoting most of our discussion.

For a one-dimensional chain the vertices and sites can be labeled as (v_i, l_i) , with i running from 1 through L for a chain of length L (see Fig. 1). Then we write the Hamiltonian

$$H = - \sum_{i=1}^L (A_i + C_i), \quad (1)$$

arXiv:2102.10812v1 [cond-mat.str-el] 22 Feb 2021

where $i = (v_i, l_i)$ stands for a combined vertex+link unit. The vertex operator A_i for the V_2/L_4 model acts on a given vertex v_i and its two adjacent links (l_{i-1}, l_i) as

$$A_i = \frac{1}{4} \sum_{n=0}^3 (X_{l_{i-1}} x_{v_i} X_{l_i}^3)^n = \frac{1}{4} (1 + X_{l_{i-1}} x_{v_i} X_{l_i}^3 + X_{l_{i-1}}^2 X_{l_i}^2 + X_{l_{i-1}}^3 x_{v_i} X_{l_i}). \quad (2)$$

The link operator C_i acts on the given link l_i and its two neighboring vertices (v_i, v_{i+1}) ,

$$C_i = \frac{1}{2} \sum_{n=0}^1 (z_{v_i} Z_{l_i}^2 z_{v_{i+1}})^n = \frac{1}{2} (1 + z_{v_i} Z_{l_i}^2 z_{v_{i+1}}). \quad (3)$$

Such choice of A and C operators is specific to the V_2/L_4 model.

The operator form of A_i depends on the direction of “arrows” on the links. The rule is to assign X to a link with an “incoming” arrow to a vertex and X^3 to a link with an “outgoing” arrow. The A -operator for arbitrary arrow directions on the links is therefore given by

$$A_i = \frac{1}{4} \sum_{n=0}^3 \left(\prod_{l_{in}} X_{l_{in}} \prod_{l_{out}} X_{l_{out}}^3 x_{v_i} \right)^n. \quad (4)$$

The products $\prod_{l_{in}}$ and $\prod_{l_{out}}$ mean, for example, that if both arrows are “in”, then we must write $(X_{l_{i-1}}^3 x_{v_i} X_{l_i}^3)^n$. For simplicity, we adhere to the arrow scheme shown in Fig. 1 and the vertex operator definition in Eq. (2).

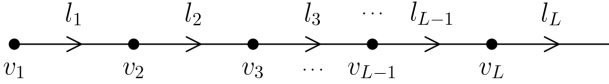


FIG. 1. Schematic figure of alternating vertices and oriented links. For a closed chain the link l_L attaches to the vertex v_1 .

The lower-case x_v and z_v operators act on the vertices. Meanwhile, upper-case X_l and Z_l operate on the link states. In general they satisfy $X_l |g\rangle_l = |g+1\rangle_l \pmod{4}$ and $Z_l |g\rangle_l = \omega^g |g\rangle_l$ with $\omega = i, g = 0, 1, 2, 3$. Similar relations hold for the vertex operators, with $\omega = -1$. An identity

$$Z_l^p X_l^q = \omega^{pq} X_l^q Z_l^p \quad (5)$$

will be used repeatedly for many of the derivations that will follow. It is easily verified that all the projectors in the Hamiltonian are mutually commuting and square to itself.

This model we wrote down in Eq. (1) possesses some global symmetries. For the V_2/L_4 Hamiltonian, there are two global symmetry operators

$$\phi = \prod_i x_{v_i}, \quad \theta = \prod_i Z_{l_i}, \quad (6)$$

which generate the $\mathbb{Z}_2 \times \mathbb{Z}_4$ symmetry of the model. One can check that both symmetry generators commute with the Hamiltonian. A crucial aspect of the V_2/L_4 model is the existence of a local \mathbb{Z}_2 operator $X_{l_i}^2$, which commutes with the Hamiltonian $[H, X_{l_i}^2] = 0$ for any link l_i . Such local operator is absent in the V_2/L_2 model. As a result, the eigenstates can be classified according to the set of quantum numbers or “ p -sectors”

$$p \equiv \{p_1, \dots, p_L\} \quad (7)$$

where $p_i = \pm 1$ stands for the eigenvalue of $X_{l_i}^2$ at the link l_i .

Within each p -sector one can reduce the V_2/L_4 model to an effective V_2/L_2 model. To accomplish this, first one organizes the link states in terms of the eigenstates of X_l :

$$\begin{aligned} |\bar{0}\rangle_l &= (|0\rangle + |1\rangle_l + |2\rangle_l + |3\rangle_l)/2, \\ |\bar{1}\rangle_l &= (|0\rangle_l + \omega^3 |1\rangle_l + \omega^2 |2\rangle_l + \omega |3\rangle_l)/2, \\ |\bar{2}\rangle_l &= (|0\rangle_l - |1\rangle_l + |2\rangle_l - |3\rangle_l)/2, \\ |\bar{3}\rangle_l &= (|0\rangle_l + \omega |1\rangle_l + \omega^2 |2\rangle_l + \omega^3 |3\rangle_l)/2. \end{aligned} \quad (8)$$

It is easily shown that

$$\begin{aligned} X_l |\bar{n}\rangle_l &= \omega^n |\bar{n}\rangle_l, \\ Z_l |\bar{n}\rangle_l &= |\bar{n-1}\rangle_l. \end{aligned} \quad (9)$$

Both $|\bar{0}\rangle_l$ and $|\bar{2}\rangle_l$ share the same eigenvalue $X_{l_i}^2 = p_i = +1$. For $|\bar{1}\rangle_l$ and $|\bar{3}\rangle_l$ the eigenvalue is $p_i = -1$. Within a given p -sector, we have

$$\begin{aligned} Z_{l_i}^2 |\bar{0}\rangle_{l_i} &= |\bar{2}\rangle_{l_i}, \quad (p_i = +1) \\ Z_{l_i}^2 |\bar{1}\rangle_{l_i} &= |\bar{3}\rangle_{l_i}, \quad (p_i = -1). \end{aligned} \quad (10)$$

In other words, the Z_l^2 operator acts effectively as a spin-1/2 Pauli operator, $Z_{l_i}^2 \rightarrow x_{l_i}$, in the two-dimensional subspace of fixed p_i . One can also show that X_{l_i} acts as the Pauli- z_{l_i} if $p_i = +1$, and as $X_{l_i} \equiv \omega z_{l_i}$ if $p_i = -1$. As a result, the following replacements are allowed in a given p -sector:

$$\begin{aligned} X_l &\rightarrow \omega^{(1-p_l)/2} z_l, \\ X_l^2 &\rightarrow p_l, \\ X_l^3 &\rightarrow p_l \omega^{(1-p_l)/2} z_l. \end{aligned} \quad (11)$$

With these considerations one can reduce the A_i and C_i operators in Eqs. (2) and (3) as

$$\begin{aligned} A_i &\rightarrow A_i^{(p)} = \frac{1}{4} \left[1 + p_{i-1} p_i \right. \\ &\quad \left. + (p_{i-1} + p_i) \omega^{-(p_{i-1} + p_i)/2 + 1} z_{l_{i-1}} x_{v_i} z_{l_i} \right] \\ C_i &\rightarrow C_i^{(p)} = \frac{1}{2} (1 + z_{v_i} x_{l_i} z_{v_{i+1}}). \end{aligned} \quad (12)$$

Each p -sector then gives rise to an effective V_2/L_2 Hamiltonian

$$H^{(p)} = - \sum_i (A_i^{(p)} + C_i^{(p)}) \quad (13)$$

with the $A_i^{(p)}$ and $C_i^{(p)}$ terms given in Eq. (12). One can view the original V_2/L_4 model as the direct sum

$$H = \oplus_p H^{(p)}, \quad (14)$$

where each $H^{(p)}$ is defined in the V_2/L_2 subspace. From Eq. (12) we obtain identical operators $A_i^{(p)}$ when all the p_i 's are reversed, $p_i \rightarrow -p_i$, implying that each V_2/L_2 sector ought to be *doubly degenerate*. The two degenerate subspaces are connected by the global operation $\prod_i Z_{l_i}$ or $\prod_i Z_{l_i}^3$, both of which implement $p_i \rightarrow -p_i$. In other words,

$$\begin{aligned} H^{(-p)} &= \left(\prod_i Z_{l_i} \right) H^{(p)} \left(\prod_i Z_{l_i}^3 \right) \\ &= \left(\prod_i Z_{l_i}^3 \right) H^{(p)} \left(\prod_i Z_{l_i} \right). \end{aligned} \quad (15)$$

In particular, the ground states of the V_2/L_4 model comes from the sector $p = \{1, \dots, 1\}$ and $p = \{-1, \dots, -1\}$ where one can write A_i and C_i as

$$\begin{aligned} A_i &= \frac{1}{2}(1 + z_{l_{i-1}} x_{v_i} z_{l_i}), \\ C_i &= \frac{1}{2}(1 + z_{v_i} x_{l_i} z_{v_{i+1}}). \end{aligned} \quad (16)$$

In fact, this V_2/L_2 model has been studied extensively as a model for one-dimensional SPT^{13,14}. The V_2/L_4 model is a natural extension of the V_2/L_2 model. The pure V_2/L_2 model, with all $p_l = 1$ or -1 , has the global $\mathbb{Z}_2 \times \mathbb{Z}_2$ symmetry generated by

$$\prod_i x_{v_i} \quad \text{and} \quad \prod_i x_{l_i}, \quad (17)$$

but no extra local symmetry.

III. GROUND STATES OF V_2/L_4 MODEL

There are two ways to go about writing down the ground states of the V_2/L_4 Hamiltonian, Eq. (1). The first one is to identify the ground states of $-\sum_i C_i$ and then act on them with the projector $\prod_i A_i$. The other way is to first identify the ground states of $-\sum_i A_i$, and then act on them with the projector $\prod_i C_i$. It is not hard to see that both ways lead to states with the eigenvalues of A_i and C_i all equal to $+1$, which by definition gives the ground states of the projector Hamiltonian.

Given our analysis in the previous section, it seems more enlightening to analyze the ground states in the eigenbasis of $X_{l_i}^2$, where the operator A_i is diagonalized easily. We obtain the two degenerate ground states of the V_2/L_4 model as

$$\begin{aligned} |G_1\rangle &= P_C |S_1\rangle, \quad |G_2\rangle = P_C |S_2\rangle \\ |S_1\rangle &= (\otimes_i |\bar{0}\rangle_{v_i}) (\otimes_j |\bar{0}\rangle_{l_j}) \\ |S_2\rangle &= (\otimes_i |\bar{0}\rangle_{v_i}) (\otimes_j |\bar{1}\rangle_{l_j}). \end{aligned} \quad (18)$$

The vertex eigenstates $|\bar{0}\rangle_{v_i} = (|0\rangle_{v_i} + |1\rangle_{v_i})/\sqrt{2}$ and $|\bar{1}\rangle_{v_i} = (|0\rangle_{v_i} - |1\rangle_{v_i})/\sqrt{2}$ diagonalize the x_v operator. The ground states of the V_2/L_4 model are obtained as the projection by $P_C = \prod_i C_i$ on the two ‘‘seed states’’ $|S_1\rangle$ and $|S_2\rangle$. The (unique) ground state of the V_2/L_2 model is obtained from $|G_1\rangle$ above, by rewriting C_i as in Eq. (16). The two ground states of the V_2/L_4 model share the properties

$$\begin{aligned} \left(\prod_i Z_{l_i} \right) |G_1\rangle &= |G_2\rangle, \\ X_{l_i}^2 |G_1\rangle &= +|G_1\rangle \\ X_{l_i}^2 |G_2\rangle &= -|G_2\rangle. \end{aligned} \quad (19)$$

We also show how to write down the ground states in the Z -basis, where the C_i 's are diagonalized first and $P_A = \prod_i A_i$ acts as a projector. The two ground states are

$$\begin{aligned} |G'_1\rangle &= P_A \left[(\otimes_i |0\rangle_{v_i}) (\otimes_j |0\rangle_{l_j}) \right], \\ |G'_2\rangle &= P_A \left[(\otimes_i |0\rangle_{v_i}) (\otimes_{j \neq j'} |0\rangle_{l_j}) \otimes |2\rangle_{l_{j'}} \right] \end{aligned} \quad (20)$$

where j' is arbitrary. These ground states share the properties

$$\begin{aligned} X_{l_i}^2 |G'_1\rangle &= |G'_2\rangle, \\ \left(\prod_i Z_{l_i} \right) |G'_1\rangle &= +|G'_1\rangle, \\ \left(\prod_i Z_{l_i} \right) |G'_2\rangle &= -|G'_2\rangle. \end{aligned} \quad (21)$$

Comparing Eqs. (19) and (21), one concludes

$$\begin{aligned} |G_1\rangle &= (|G'_1\rangle + |G'_2\rangle)/\sqrt{2} \\ |G_2\rangle &= (|G'_1\rangle - |G'_2\rangle)/\sqrt{2}. \end{aligned} \quad (22)$$

In what follows, we provide a geometrical interpretation of the ground state $|G_1\rangle$. Due to $z_v^2 = 1$, the product of neighboring $z_{v_i} z_{v_{i+1}}$ is simply $Q_{12} = z_{v_1} (\prod_{i \in \mathcal{S}} z_{l_i}^2) z_{v_2}$ where $i \in \mathcal{S}$ stands for the links between the left-most vertex v_1 and the right-most one v_2 . Its action on the seed state $|S_1\rangle$ permutes the link states along \mathcal{S} , i.e., $|\bar{0}\rangle_l \rightarrow |\bar{2}\rangle_l$ and flips the vertex states at edges $|\bar{0}\rangle_{v_{1/2}} \rightarrow |\bar{1}\rangle_{v_{1/2}}$, or graphically illustrated as

$$Q_{12} |S_1\rangle = \text{Diagram: A circle with two vertices labeled } v_1 \text{ and } v_2 \text{ on the bottom. A blue dot is on the edge between } v_1 \text{ and } v_2. \text{ A red string connects } v_1 \text{ and } v_2 \text{ along the top arc.}$$

where blue dot stands for each edge vertex while the red string for all links and vertices along \mathcal{S} . Consequently, the expansion of the projector P_C leads to the superposition of all possible string configurations on the circle:

$$|G_1\rangle = \text{Diagram: A circle with no string} + \text{Diagram: A circle with a red string and a blue dot} + \text{Diagram: A circle with a red string and two blue dots} + \dots + \text{Diagram: A circle with a red string and many blue dots.} \quad (23)$$

Due to $|G_2\rangle = \prod_i Z_{l_i} |G_2\rangle$, the geometrical interpretation of $|G_2\rangle$ is given in the same manner. Only difference is that all link states are raised by one, i.e., $|\bar{n}\rangle_l \rightarrow |\bar{n} + 1\rangle_l$.

In an open chain of the same model, some edge states appear as a consequence of SPT, as thoroughly analyzed in Ref. 19.

IV. V_2/L_4 MODEL ON A GRAPH

A. GSD on a Graph

The discussion of the ground states of the V_2/L_4 model both in the closed and the open chain thus far might suggest that we are merely dealing with what seems to be two copies of the well-known V_2/L_2 model. Interestingly, the real point of departure between the two families of models occurs when these models are put on a *graph*¹⁹. The closed circle is a simplest example of a graph with the first Betti number $B_1 = 1$. Now, one can imagine putting the model on a more intricate graph such as shown in Fig. 2(b), which has $B_1 = 2$. Intuitively, the first Betti number measures the number of *cycles* or independent loops in a given graph.

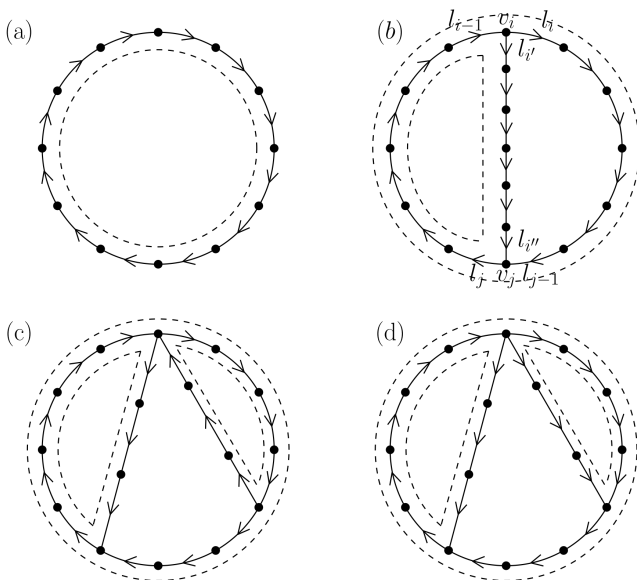


FIG. 2. Examples of closed and connected planar graphs with various Betti numbers (a) $B_1 = 1$, (b) $B_1 = 2$, and (c), (d) $B_1 = 3$. Dots are the vertices and the arrows represent the links of the graph. Dashed lines are the independent closed loops where we can perform a subsystem \mathbb{Z}_4 symmetry transformation. Because of the orientation, the loop operators correspond to the right semi-circular loop are different for (c) and (d).

Considering a $B_1 = 2$ graph such as shown in Fig. 2(b), one can write the same A_i and C_i projectors as in the $B_1 = 1$ graph, namely a circle, except at the two vertices v_i and v_j where two lines become connected at the vertex. At these vertices, there are three (not two) links which

are connected to a single vertex. The definition of the vertex operators which are projectors and commute with other vertex operators must generalize accordingly,

$$\begin{aligned} A_i &= \frac{1}{4}(1 + X_{l_{i-1}} X_{l_i}^3 X_{l_i'}^3 x_{v_i} \\ &\quad + X_{l_{i-1}}^2 X_{l_i}^2 X_{l_i'}^2 + X_{l_{i-1}}^3 X_{l_i} X_{l_i'} x_{v_i}) \\ A_j &= \frac{1}{4}(1 + X_{l_{j-1}} X_{l_j}^3 X_{l_j''}^3 x_{v_j} \\ &\quad + X_{l_{j-1}}^2 X_{l_j}^2 X_{l_j''}^2 + X_{l_{j-1}}^3 X_{l_j} X_{l_j''} x_{v_j}) \end{aligned} \quad (24)$$

where v_i (v_j) has one (two) arrowhead towards it and two (one) arrowheads away from it. In fact, a completely general definition of the vertex operator for arbitrary graph is possible as

$$A_i = \frac{1}{4} \sum_{j=0}^3 \left[\left(\prod_{q \in \text{in}} X_{l_{q,i}} \prod_{q' \in \text{out}} X_{l_{q',i}}^3 \right) x_{v_i} \right]^j. \quad (25)$$

There is a factor X (X^3) for the links whose arrows come into (out of) the vertex. The link operator C_i is the same as in Eq. (3) regardless of the graph type. Despite the much complex forms, A_i and C_j always remain mutually commuting projectors. The V_2/L_4 Hamiltonian on an arbitrary graph generalizes accordingly,

$$H = - \sum_{i=1}^{N_v} A_i - \sum_{j=1}^{N_l} C_j, \quad (26)$$

spanning all the vertices and the links in the graph and using Eq. (25) for the vertex operator. The number of vertices (N_v) and of links (N_l) are no longer equal for a general graph but are rather related by the first Betti number,

$$N_l - N_v + 1 = B_1. \quad (27)$$

B. Subsystem Symmetries

We can discuss how to explicitly construct the multitude of degenerate ground states on a graph. For example, the V_2/L_4 model defined on a graph shown in Fig. 2(b) allows two loop operators that commute with the Hamiltonian. We call them θ_1 and θ_2 , and they consist of the product of Z_l 's along the left semi-circular loop and the large circular loop, respectively. These two loops are drawn as dashed lines in Fig. 2(b). Note that the definition of these loop operators are obtained by simply “following the arrows” drawn on the graph. On a $B_1 = 2$ graph we have two such independent loops. Accordingly one can write down four independent ground states, which are $|G_1\rangle = P_C [(\otimes_i |\bar{0}\rangle_{v_i}) (\otimes_j |\bar{0}\rangle_{l_j})]$, and

$$\begin{aligned} |G_2\rangle &= \theta_1 |G_1\rangle, \\ |G_3\rangle &= \theta_2 |G_1\rangle, \\ |G_4\rangle &= \theta_1 \theta_2 |G_1\rangle. \end{aligned} \quad (28)$$

At first sight the construction of degenerate ground states on a graph bears resemblance to the way that topologically distinct states are generated on a finite-genus space. The GSD formula $\text{GSD} = 2^{B_1}$ has resemblance to the formula for the topological GSD $= 2^{2g}$, which applies to *two-dimensional* topological models such as the toric code, where g (also known as the second Betti number) is the genus of two-dimensional surface.

Unlike the topologically ordered states which do not have local order parameters, the four ground states derived above can be distinguished by their “order parameter” X_l^2 . With $|G_1\rangle$, the expectation value is $\langle G_1 | X_l^2 | G_1 \rangle = +1$ on every link of the graph. For $|G_2\rangle$, the links along the loop where θ_1 acts have $\langle X_l^2 \rangle = -1$. For $|G_3\rangle$, it is the links along the outer perimeter where the order parameters are reversed. Finally in the fourth ground state $|G_4\rangle$ it is the other inner loop where the links have $\langle X_l^2 \rangle = -1$. The four order parameter patterns are depicted in Fig. 3. There is a clear parallel to the usual classification of states by order parameters, but one must carefully note that its nature is not entirely global. Perhaps a better terminology is the *subsystem symmetry breaking* (SSB, not to be confused with the *spontaneous symmetry breaking*) and distinguish it from the global symmetry breaking (GSB) of most many-body models.

Along a similar line of reasoning, the loop operator consisting of the product of Z_i 's and Z_i^3 's along the independent loops as dictated by the flow of arrows commute with the Hamiltonian and performs the *subsystem \mathbb{Z}_4 symmetry transformation*. In the case of Fig. 2(c), all such loop operators consist of the product of Z_i 's only. On the other hand, the loop operator corresponding to the right semi-circular loop in Fig. 2(d) is $\prod_i Z_{l_i} \prod_{i'} Z_{i'}^3$, where i 's are the links on the arc and i' 's are the links on the inner segment. The number of independent loops equals the Betti number B_1 , and the degenerate ground states are generated by applying the subsystem loop operators and their products on one particular ground state $|G\rangle$. There are exactly $2^{B_1} - 1$ different products of subsystem loop operators available, for a total of 2^{B_1} ground states on a graph with the Betti number B_1 .

The V_2/L_4 Hamiltonian on a graph still has the exact symmetry $[H, X_l^2] = 0$ for all the links l . As a result, X_l^2 operators in the graph model can be replaced by their respective quantum numbers p_l . In particular, the vertex operators at the junction given in Eq. (24) become, in a given p -sector,

$$\begin{aligned} A_i^{(p)} &= \frac{1}{4} [1 + p_{i-1} p_i p_{i'} \\ &\quad + (p_i p_{i'} + p_{i-1}) \omega^{(3-p_{i-1}-p_i-p_{i'})/2} z_{l_{i-1}} z_{l_i} z_{l_{i'}} x_{v_i}] \\ A_j^{(p)} &= \frac{1}{4} [1 + p_{j-1} p_j p_{j'} \\ &\quad + (p_{j-1} p_{j'} + p_j) \omega^{(3-p_{j-1}-p_j-p_{j'})/2} z_{l_{j-1}} z_{l_j} z_{l_{j'}} x_{v_j}]. \end{aligned} \quad (29)$$

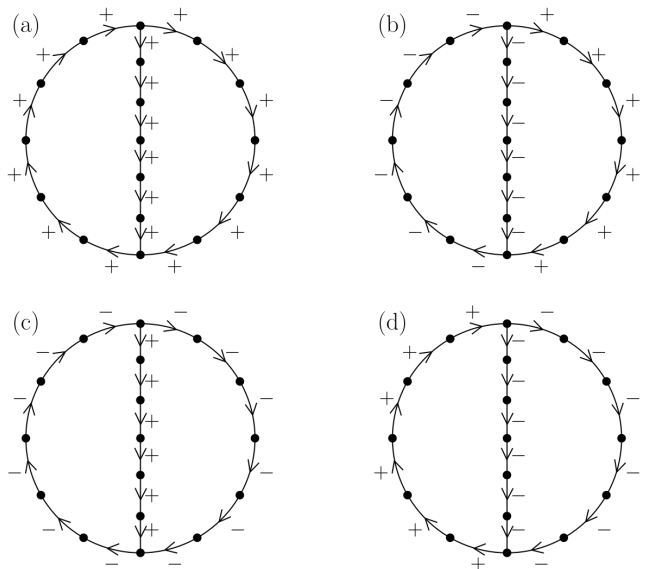


FIG. 3. Four kinds of configurations of p 's that reduce the V_2/L_4 model to the V_2/L_2 model when $B_1 = 2$. The \pm signs on the links represent the eigenvalues of X_l^2 , or equivalently, the p_l 's.

One can show, by explicit calculation, that $A_i^{(p)}$ becomes $\frac{1}{2}(1 + z_{l_{i-1}} z_{l_i} z_{l_{i'}} x_{v_i})$ for $\{p_{i-1}, p_i, p_{i'}\} = \{1, 1, 1\}, \{-1, 1, -1\}, \{-1, -1, 1\}$. In a similar manner, we have $A_j^{(p)} = \frac{1}{2}(1 + z_{l_{j-1}} z_{l_j} z_{l_{j'}} x_{v_j})$ for $\{p_{j-1}, p_j, p_{j'}\} = \{1, 1, 1\}, \{-1, -1, 1\}, \{1, -1, -1\}$. The V_2/L_2 model on a graph comes from having the following choice of vertex operators:

$$\begin{aligned} A_i^{(p)} &= \frac{1}{2}(1 + z_{l_{i-1}} z_{l_i} z_{l_{i'}} x_{v_i}) \\ A_j^{(p)} &= \frac{1}{2}(1 + z_{l_{j-1}} z_{l_j} z_{l_{j'}} x_{v_j}) \end{aligned} \quad (30)$$

at the two junctions i and j shown in Fig. 2(b). For all other vertices and all the links one has the usual definition of the vertex and link operators given in Eq. (16). After some enumeration, one finds the four configurations of p 's shown in Fig. 3 can reduce the V_2/L_4 model to the V_2/L_2 model on the graph with $B_1 = 2$. This argument again shows why there is fourfold degeneracy of the ground states on the $B_1 = 2$ graph.

It is worth examining the general character of the pure V_2/L_2 model on a graph. It can be shown that GSD of the V_2/L_2 model remains at GSD=1 regardless of the Betti number of the graph. The global $\mathbb{Z}_2 \times \mathbb{Z}_2$ symmetry of the V_2/L_2 model on a simply connected graph with $B_1 = 1$ is partially lost due to the vertex terms at the junction, Eq. (30). One can prove quite easily that although $\prod_i x_{v_i}$ remains a symmetry, $\prod_i x_{l_i}$ no longer commutes with the vertex operators at the junction and hence fails to be a symmetry operator. The global symmetry of the V_2/L_2 model is lowered from $\mathbb{Z}_2 \times \mathbb{Z}_2$ to \mathbb{Z}_2 on a multiply connected graph. On further observation, however, we realize that a *partial* product of link

operators $\prod'_i x_{l_i}$ for the links forming a closed loop *does commute* with the junction terms in Eq. (30) and restore the $\mathbb{Z}_2 \times \mathbb{Z}_2$ symmetry for that loop. Contrasted with the usual SPT, this is a realization of the subsystem SPT, or SSPT¹⁵. By implication, when we cut open any segment of the graph, the emerging edge behavior and symmetry fractionalization will be exactly those of the open chain case already analyzed. Since the ground states of the pure V_2/L_2 model are ground states of the V_2/L_4 model, even in V_2/L_4 model there is SSPT.

V. EXCITATIONS

The concept of excitation arises naturally in frustration-free models to which our V_2/L_4 model belongs. The ground state(s) has all of the eigenvalues of A_i and C_i equal to +1, and excited states should have one of these equal to zero instead¹⁹. Depending on whether the link or the vertex operator eigenvalues change from 1 to 0, one can make a distinction between link excitations and vertex excitations. Another useful way to classify excitations is in terms of the changes in the p -eigenvalues, $p = \{p_1, \dots, p_L\}$, of the chain. Changes in any of the eigenvalues in the p -set leads to different sectors of the block, $H = \oplus_p H^{(p)}$, where H is the original V_2/L_4 Hamiltonian and each $H^{(p)}$ represents some realization of the V_2/L_2 Hamiltonian. We will examine the nature of excitations from both perspectives. Eigenvalues of A_i and C_i will be denoted a_i and c_i from now on.

The link excitation is attained by rewriting one of the operators C_i in the projector P_C by its orthogonal complement¹⁹

$$C_i^\perp = \frac{1}{2}(1 - z_{v_i} Z_{l_i}^2 z_{v_{i+1}}), \quad C_i^\perp C_i = 0. \quad (31)$$

We can define the projector

$$P_C(j) = \left(\prod_{i < j} C_i \right) C_j^\perp \left(\prod_{i > j} C_i \right), \quad (32)$$

and use such projector to create a link-excited state

$$|l_j\rangle = P_C(j)|S\rangle \quad (33)$$

with $|S\rangle$ being one of the two seed states. Since $C_j|l_j\rangle = 0$, one concludes $c_j = 0$, qualifying it as a link excitation. Note that $X_{l_j} C_j = C_j^\perp X_{l_j}$, and therefore

$$\begin{aligned} X_{l_j}|G\rangle &= X_{l_j} P_C|S\rangle = P_C(j) X_{l_j}|S\rangle \\ &= \pm P_C(j)|S\rangle = \pm |l_j\rangle, \end{aligned} \quad (34)$$

where the \pm sign comes from having $|S\rangle = |S_1\rangle$ or $|S\rangle = |S_2\rangle$. In other words, link excitations are created by applying X_{l_i} on a given link to the ground states. By a similar consideration, we learn that x_{v_j} acting on the ground states generate a link-pair excitation:

$$x_{v_j}|G\rangle = |l_{j-1}, l_j\rangle. \quad (35)$$

The proof comes from the observation,

$$x_{v_j} P_C = \left(\prod_{i < j-1} C_i \right) C_{j-1}^\perp C_j^\perp \left(\prod_{i > j+1} C_i \right). \quad (36)$$

A string of x -excitations acting on the ground states gives

$$x_{v_2} \cdots x_{v_k} |G\rangle = |l_1, l_k\rangle \quad (37)$$

and when the string forms a closed loop, the state gets back to the original ground state, e.g. $\prod_{i \in \text{loop}} x_{v_i} |G\rangle = |G\rangle$.

Both types of link-excited states $X_{l_j}|G\rangle$ and $x_{v_j}|G\rangle$ share the same p -eigenvalues as the ground state. This is seen by the fact that the operator that defines the p -eigenvalue, X_l^2 , commutes with X_l and x_v which create the link excitations. We conclude that the link excitations $X_{l_j}|G\rangle$ and $x_{v_j}|G\rangle$ occurs in the same p -sector as the ground state (intra- p excitation). In this regard, the link excitations we write down here are the same as what the V_2/L_2 model would give.

The p -altering or inter- p excitations are created by acting with Z_{l_j} directly on the seed states. Since Z_{l_i} commutes with the projector P_C , the p -altering excited state is given by

$$P_C(Z_{l_j}|S\rangle) = Z_{l_j}|G\rangle. \quad (38)$$

One can easily check that $X_{l_j}^2$ anti-commutes with Z_{l_j} , therefore p_{l_j} changes from +1 to -1. This state, interestingly, continues to remain an eigenstate of C_i with $c_i = +1$ everywhere. Contrary to naive expectation, $Z_{l_j}|G\rangle$ is *not* a link excitation. When one applies A_i to this state, some nontrivial changes are discovered:

$$\begin{aligned} A_j Z_{l_j} &= \frac{1}{4} Z_{l_j} (1 + \omega^3 X_{l_{j-1}} x_{v_j} X_{l_j}^3 \\ &\quad + \omega^2 X_{l_{j-1}}^2 X_{l_j}^2 + \omega X_{l_{j-1}}^3 x_{v_j} X_{l_j}) \\ A_{j+1} Z_{l_j} &= \frac{1}{4} Z_{l_j} (1 + \omega X_{l_j} x_{v_{j+1}} X_{l_{j+1}}^3 \\ &\quad + \omega^2 X_{l_j}^2 X_{l_{j+1}}^2 + \omega^3 X_{l_j}^3 x_{v_{j+1}} X_{l_{j+1}}). \end{aligned} \quad (39)$$

The appearance of new terms on the right side of the equations necessitates that we define some new vertex projectors as follows:

$$\begin{aligned} A_i(n) &= \frac{1}{4} (1 + \omega^n X_{l_{i-1}} x_{v_i} X_{l_i}^3 \\ &\quad + \omega^{2n} X_{l_{i-1}}^2 X_{l_i}^2 + \omega^{3n} X_{l_{i-1}}^3 x_{v_i} X_{l_i}). \end{aligned} \quad (40)$$

The vertex projector used to define the Hamiltonian is recovered for $n = 0$, and the relations derived in Eq. (39) are now succinctly summed up:

$$\begin{aligned} A_j Z_{l_j} &= Z_{l_j} A_j(3) \\ A_{j+1} Z_{l_j} &= Z_{l_j} A_{j+1}(1). \end{aligned} \quad (41)$$

The $A_i(n)$ projectors commute with C_j and $A_i(n)A_i(n') = 0$ unless $n = n'$. Furthermore, $A_i(n)|S\rangle = 0$ unless $n = 0$. Due to these properties, we can show

$$A_j Z_{l_j} |G\rangle = A_{j+1} Z_{l_j} |G\rangle = 0. \quad (42)$$

In other words, a pair of vertex excitations with $a_j = a_{j+1} = 0$ has been created. We conclude that different p -sectors of the V_2/L_4 model are connected through the creation of vertex-pair excitations. A $p_{l_j} = 1 \rightarrow -1$ implies that a pair of adjacent vertices have been excited, $a_j = a_{j+1} = 0$. We may sum up the situation as

$$\begin{aligned} Z_{l_j} |G\rangle &= |\omega_{v_j}^3, \omega_{v_{j+1}}\rangle, \\ Z_{l_j}^3 |G\rangle &= |\omega_{v_j}, \omega_{v_{j+1}}^3\rangle. \end{aligned} \quad (43)$$

The symbol on the right $|\omega_v^n\rangle$ means that the seed state has been acted on by $A_v(n)$ before the projector P_C is applied. The vertex excitations carrying ω^3 and ω as quantum numbers must exist as a pair, and serve to connect different p -sectors.

On the other hand, exciting the vertex state by z_v or a link state by Z_l^2 does not change the p -eigenvalues, and leads to the following excitations:

$$\begin{aligned} z_{v_j} |G\rangle &= |\omega_{v_j}^2\rangle, \\ Z_{l_j}^2 |G\rangle &= |\omega_{v_j}^2, \omega_{v_{j+1}}^2\rangle = z_{v_j} z_{v_{j+1}} |G\rangle. \end{aligned} \quad (44)$$

The vertex excitation with the quantum number $\omega^2 = -1$ can exist in isolation. The link projector C_i has the useful identity $C_j = z_{v_j} z_{v_{j+1}} Z_{l_j}^2 C_j$, which one can verify directly from its definition. As a result, P_C acting on some seed state $|S\rangle$ leads to the same consequence as when acting on a different seed state $z_{v_j} z_{v_{j+1}} Z_{l_j}^2 |S\rangle$. This leads to the identity mentioned in the second equation above.

The p -changing vertex-pair excitation created by $Z_{l_j} |G\rangle$ can be generalized by considering a string of Z -excitations given by the product

$$Z_{l_1} \cdots Z_{l_k} |G\rangle = |\omega_{v_1}^3, \omega_{v_{k+1}}\rangle. \quad (45)$$

By the time the product $\prod_i Z_{l_i}$ forms a closed loop, one reaches the other ground state, e.g. $(\prod_{i \in \text{loop}} Z_{l_i}) |G_1\rangle = |G_2\rangle$. To sum up, there are intra- p excitations in the form of link excitations [Eq. (34)] and vertex excitations [Eq. (44)], and inter- p excitations in the form of vertex-pair excitations [Eq. (43)]. This gives the complete classification of the elementary excitations in the V_2/L_4 model.

VI. DISCUSSION

In this paper we have analyzed the properties of the V_2/L_4 model on a general graph¹⁹. The Hilbert space of the model is block-diagonalized by a set of local quantum numbers $\{p_{l_i} = \pm 1\}$, and we have shown that the V_2/L_4 model maps to a general V_2/L_2 model in each p -sector.

The GSD of our model grows exponentially with the Betti number B_1 characterizing the number of cycles in a graph. In fact one can easily show that the exponential growth of GSD with the Betti number is not unique to the V_2/L_4 model. Even a simple Potts model on a graph can be defined in a way that exhibits the same GSD behavior. For that, one considers the same kind of graph as before and place n degrees of freedom at each link labeled by the variable $z_l = 0, \dots, n-1$, and none on the vertices. We then have the Potts interaction $-\delta_{z_l, z_{l'}}$ for the neighboring links (l, l') , except when more than two lines meet at a vertex. In that case we have the three-link interaction $-\delta_{z_{l_1}, z_{l_2}, z_{l_3}}$ among the three links (l_1, l_2, l_3) joined at a vertex. For more than three links, one simply takes the delta function of all the links $-\delta_{z_{l_1}, z_{l_2}, \dots}$ with an overall minus sign. It is easily verified that the ground states have the z_l 's distributed in exactly the same pattern as those of X_l^2 's (or p_l 's) shown in Fig. 3 when $n = 2$. For general graphs and n degrees of freedom, GSD equals n^{B_1} , but no feature of SPT or symmetry fractionalization would be present in such models.

To sum up, the subsystem symmetry and its breaking observed in the V_2/L_4 model is not related to the SPT nature of the phase but rather co-exist with it. The idea of subsystem symmetries is applicable for both the Landau order parameter characterized by X_l^2 , and the SPT order.

ACKNOWLEDGMENTS

H. J. H. was supported by the Quantum Computing Development Program (No. 2019M3E4A1080227). H.-Y.L. was supported by a Korea University Grant and National Research Foundation of Korea (NRF-2020R1I1A3074769). We appreciate enlightening discussion with Munjip Park.

* Electronic address: hanjemme@gmail.com

¹ V. Kalmeyer and R. B. Laughlin, Phys. Rev. Lett. **59**, 2095 (1987).

² X. G. Wen, F. Wilczek, and A. Zee, Phys. Rev. B **39**, 11413 (1989).

³ A. Y. Kitaev, Physics-Uspekhi **44**, 131 (2001).

⁴ X. Chen, Z.-C. Gu, and X.-G. Wen, Phys. Rev. B **82**, 155138 (2010).

⁵ X. Chen, Z.-C. Gu, and X.-G. Wen, Phys. Rev. B **83**, 035107 (2011).

⁶ X. Chen, Z.-C. Gu, Z.-X. Liu, and X.-G. Wen, Phys. Rev. B **87**, 155114 (2013).

⁷ N. Schuch, D. Pérez-García, and I. Cirac, Phys. Rev. B **84**, 165139 (2011).

⁸ F. Pollmann, A. M. Turner, E. Berg, and M. Oshikawa, Phys. Rev. B **81**, 064439 (2010).

⁹ F. Pollmann, E. Berg, A. M. Turner, and M. Oshikawa, Phys. Rev. B **85**, 075125 (2012).

¹⁰ F. Pollmann and A. M. Turner, Phys. Rev. B **86**, 125441 (2012).

¹¹ D. V. Else and C. Nayak, Phys. Rev. B **90**, 235137 (2014).

- ¹² R. Bondesan and T. Quella, *Journal of Statistical Mechanics: Theory and Experiment* **2013**, P10024 (2013).
- ¹³ X. Chen, Y.-M. Lu, and A. Vishwanath, *Nature Communications* **5**, 3507 (2014).
- ¹⁴ S. D. Geraedts and O. I. Motrunich, “Exact models for symmetry-protected topological phases in one dimension,” (2014), arXiv:1410.1580 [cond-mat.stat-mech].
- ¹⁵ Y. You, T. Devakul, F. J. Burnell, and S. L. Sondhi, *Phys. Rev. B* **98**, 035112 (2018).
- ¹⁶ M. J. B. Ferreira, P. Padmanabhan, and P. Teotonio-Sobrinho, *Journal of Physics A: Mathematical and Theoretical* **47**, 375204 (2014).
- ¹⁷ M. J. B. Ferreira, J. P. I. Jimenez, P. Padmanabhan, and P. T. Sobrinho, *Journal of Physics A: Mathematical and Theoretical* **48**, 485206 (2015).
- ¹⁸ J. P. Ibieta-Jimenez, M. Petrucci, L. Q. Xavier, and P. Teotonio-Sobrinho, *Journal of High Energy Physics* **2020**, 167 (2020).
- ¹⁹ P. P. et al, “Frustration-free hamiltonian with topological order on graphs,” (2020), arXiv:2012.04929 [cond-mat.str-el].